Experimental Neurology 235 (2012) 357–367

Contents lists available at SciVerse ScienceDirect

Experimental Neurology

journal homepage: www.elsevier.com/locate/yexnr

Cuprizone-induced demyelination in the rat cerebral cortex and thyroid hormone effects on cortical remyelination

Lucas Silvestroff, Sandra Bartucci, Juana Pasquini, Paula Franco *

Departamento de Química Biológica e Instituto de Química y Fisicoquímica Biológicas (IQUIFIB-CONICET) Facultad de Farmacia y Bioquímica, UBA. Junín 956, CABA (C1113AAD), Buenos Aires, Argentina

ARTICLE INFO

Article history:
Received 3 November 2011
Revised 25 January 2012
Accepted 29 February 2012
Available online 7 March 2012

Keywords:
Cuprizone
Cortical demyelination
Oligodendrocytes
Thyroid hormone
Multiple sclerosis

ABSTRACT

Multiple Sclerosis (MS) is an inflammatory demyelinating disease of the Central Nervous System which is characterized by multifocal demyelinated lesions dispersed throughout the brain. Although white matter lesions have been the most extensively studied, cortical demyelinaton lesions are also detected in MS brains. Cuprizone (CPZ)-induced demyelination in rodents has been widely used as a model for MS. Most of these studies focus on oligodendrocyte-rich structures, such as the corpus callosum (CC) and the cerebellar peduncles. However, it has been recently described that CPZ administration in mice also produces cortical demyelination, resembling some of the lesions found in MS patients. In this work we used CPZ-demyelinating model in Wistar rats to study demyelination in cortical forebrain areas. At the ultrastructural level, demyelination in the cortex was observed before detectable myelin loss in the subcortical white matter. During the course of CPZ intoxication Myelin Basic Protein immunodetection was decreased in cortical layers I–III due to a reduction in the number of cortical oligodendrocytes (OL). Oligodendroglial loss in CPZ-intoxicated rats correlated with an increase in the number of Glial Fibrillary Acidic Protein positive astrocytes and a shift in the location of Carbonic Anhydrase II from OL to astrocytes. After removal of CPZ from the diet, we evaluate intranasal Thyroid hormone (TH) effects on the progression of cortical lesions. As previously reported in the CC, TH treatment also accelerates remyelination rate in the cortex compared to rats undergoing spontaneous remyelination. Our results suggest that manipulation of TH levels could be considered as a strategy to promote remyelination process in the cortex and to prevent neuronal irreversible damage in patients suffering from MS.

Introduction

Multiple Sclerosis (MS) is an immune-mediated disorder of the central nervous system (CNS). Based on the disease course MS can be classified into four groups. The most frequent relapsing-remitting form of MS (RR-MS), with alternated episodes of neurological disability and recovery, mainly displays generalized inflammatory demyelination. Primary or secondary-progressive MS patients (PP-MS or SP-MS, respectively) exhibit a steady neurological decline, associated to cortical demyelination and axonal degeneration (Polman et al., 2005, 2011). A small minority of patients are classified as progressive-relapsing MS (PR-MS) which undergo a progressive neurological decline and sporadic acute attacks (Dutta and Trapp, 2011). During the disease progression, myelin destruction and oligodendroglial loss are accompanied by loss of blood–brain-barrier (BBB) indemnity, multifocal inflammation, microglial activation, astrogliosis and axonal degeneration, all together leading to irreversible neurological disability (Dutta and Trapp, 2007; Trapp and Nave, 2008). The identification of white matter demyelinated plaques is one of the main pathological findings in MS patients. However, extensive demyelination has also been detected in cortical gray matter areas of postmortem brains (Bo et al., 2003a, 2003b; Kutzelnigg and Lassmann, 2005; Kutzelnigg et al., 2005). Severe neuronal and axonal pathologies are prominent features of cortical demyelination, which seem to occur without significant participation of immune cells from the blood, nor microglial activation (Peterson et al., 2001). Cortical lesions have been classified depending on their location (Dutta and Trapp, 2011; Peterson et al., 2001). In type I lesions, demyelination occurs in the leukocortical junction affecting both white and gray matter. Type II lesions are small perivascular demyelinated regions. Type III lesions are subpial demyelinated plaques which extend up to layers III or IV of the brain neocortex. Although an association between the lesion location and the course of the disease is not clearly established, cortical damage correlates with both motor and sensory deficits that lead to cognitive and executive dysfunction, and the characteristic

* Corresponding author at: Departamento de Química Biológica e Instituto de Química y Fisicoquímica Biológicas (IQUIFIB-CONICET) Facultad de Farmacia y Bioquímica, UBA. Junín 956, CABA (C1113AAD), Buenos Aires, Argentina.
E-mail addresses: lsilver81@yahoo.com.ar (L. Silvestroff), sandritabartuk@hotmail.com (S. Bartucci), jpasquin@qb.ffyb.uba.ar (J. Pasquini), pgfranco@ffyb.uba.ar (P. Franco).

0014-4886/$ – see front matter © 2012 Elsevier Inc. All rights reserved.
doi:10.1016/j.expneurol.2012.02.018

neurological decline that is normally found in MS patients (Calabrese et al., 2009; Rinaldi et al., 2010; Vucic et al., 2011).

Demyelination can be experimentally induced in rodents by different strategies, including experimental allergic encephalomyelitis (EAE), viral infection, physical injury or toxin exposure (Franklin, 2003). In this last group, cuprizone (CPZ) intoxication has been widely used to study the mechanisms controlling the progression of demyelination and constitutes an excellent tool for testing therapeutic interventions. As well as in MS, CPZ intoxication in rodents induces oligodendrocyte (OL) degeneration and myelin loss along with microglial activation and astrogliosis (Adamo et al., 2006; Franco et al., 2008; Hiremath et al., 1998; Komoly, 2005; Love, 1988; Ludwin, 1978; Mason et al., 2004; Stidworthy et al., 2003). Most studies have focused on white matter enriched brain structures, as the corpus callosum (CC) and cerebellar peduncles. However, CPZ also induces gray matter demyelination, as demonstrated in mice (Gudi et al., 2009; Silvestroff et al., 2010). Even though the presence of cortical lesions has been demonstrated after EAE induction in certain strains of rats (Storch et al., 2006) it is still not known whether cortical demyelination also occurs in the rat CPZ model.

In rodents, different treatments have proven to be successful in promoting/improving/accelerating remyelination after acute demyelination (reviewed by Franklin and ffrench-Constant, 2008). In particular, thyroid hormones (TH) have been shown to improve remyelination in different MS experimental models (Calzà et al., 2005, 2010; Calzà et al., 2002; Fernandez et al., 2004a; Franco et al., 2008; Harsan et al., 2008). The aim of this study is to characterize cortical demyelination in CPZ-intoxicated Wistar rats and to determine whether intranasal delivery of TH can be used to promote cortical remyelination. The data presented in this work shows that the CPZ rat model reproduces some features of type III cortical lesions found in MS brains. Thirty five day old CPZ-intoxicated rats showed a marked depletion of Myelin Basic Protein (MBP) from cortical layers I–III. We found that demyelination correlates with a reduction in the numbers of cortical OL and generalized astrogliosis. Microglia and macrophage marker CD68 was rarely detected in the cortex of control or CPZ-intoxicated rats. Despite cortical OL loss, Carbonic anhydrase isoform II (CAII), which is expressed in control brain OLs, was activated in $GFAP^+$ protoplasmic astrocytes in most affected cortical layers of CPZ-animals. Furthermore, ultrastructural analysis revealed that cortical CPZ-induced demyelination precedes subcortical white matter damage. After CPZ withdrawal from the diet, TH intranasal administration improved remyelination in the cortex compared to saline treated controls. Our results demonstrate that cortical damage is an early consequence of CPZ-induced demyelination that could serve as a model of the MS cortical pathology and highlights the critical role played by THs in cortical remyelination process. Thyroid hormone administration could represent an effective therapeutical approach for demyelinating diseases.

Material and methods

Reagents

Ketamine Chlorhidrate Base (50 mg/ml) was purchased from Holliday-Scott S.A. and 20 mg/ml Xilazine Chloridrate (Kenzol®) from Köning. Bisbenzamida H 33258 (Höechst), t-Octylphenoxypolyethoxyethanol (Triton X-100), Paraformaldehyde (PFA), tri-yodo tyronine (T3) and bis cyclohexanone oxaldhydrazone (Cuprizone) were from Sigma (Argentina). Glycerol, NaCl, and Sucrose were purchased from Biopack. Mowiol® 4–88 Reagent was purchased from Calbiochem.

Animals

Albino Wistar rats were housed under 12 hour light/12 hour dark cycles. All animal procedures were performed following the guidelines established by the Hygiene and Security Service and The Ethics Committee for the use of laboratory animals of the Science and Technology Department, School of Pharmacy and Biochemistry, Buenos Aires University, according to the Biological and Chemical Risk Prevention Manual guidelines (Res. D 8386/08).

Cuprizone induced demyelination and T3 treatment

All the animals were housed with their mothers from birth until weaning. Rats were weaned at 21 days of age and were fed with pulverized regular chow pellets supplemented with 0.6% cuprizone (CPZ) for 2 weeks to trigger demyelination. A group of control animals was subjected to a CPZ-free diet. At 35 days of age, some control (C_{35}) and CPZ-demyelinated (D_{35}) rats were sacrificed. Siblings were returned to a regular CPZ-free pellet diet and were subdivided in two groups; half received saline solution (SS) while others received T3 doses. Saline- and T3-instillated rats were sacrificed at 42 days of age. Intranasal T3 treatment was performed on days 35, 37 and 39 by holding animals face upwards for the administration of 25 μg T3 per nostril in a volume of 2.5 μl each (C_{35}–$T3_{42}$ or D_{35}–$T3_{42}$). Some animals received equal volumes of saline solution via intranasal instillation (0.9% NaCl in water) for control treatment (C_{35}–SS_{42} or D_{35}–SS_{42}). For immunohistochemical analysis, animals from different experimental groups were anesthetized with 100 μl of a Ketamine: Xilazine 3:1 mixture and sacrificed at 35 or 42 days of age by PBS (8 g/L NaCl, 0.2 g/L KCl, 0.24 g/L KH_2PO_4, 1.44 g/L Na_2HPO_4, pH 7.4) and 4% PFA intracardiac perfusion. Brains were removed, post fixed in 4% PFA overnight and rinsed with PBS. Brains were sequentially soaked in 15% and 30% sucrose solutions for 24 h in each solution at 4 °C, and finally stored at −80 °C. Coronal 20 μm thick cryosections were collected in 50% glycerol solution and stored at −20 °C.

Immunohistochemistry (IHQ)

Coronal brain slices between − 0.3 mm and + 1.4 mm from bregma according to Paxinos and Watson's stereotaxic atlas (Paxinos and Watson, 1986) were washed twice in PBS and soaked in blocking solution (5% Fetal Calf Serum (FCS), 0.1% Triton X100) for 2 h. They were then incubated o/n at 4 °C in a PBS solution containing 1% FCS, 0.1% Triton X-100 and primary antibody. We used the following dilutions of primary antibodies against MBP 1:100 (gift from Dr. A. Campagnoni, UCLA) for myelin, CC1 monoclonal antibodies (1:250) for Adenomatous Poliposis coli (APC) (Calbiochem, San Diego, CA) and anti CAII antibodies (1:200) (gift from Dr. W. Cammer) for OLs, anti Glial Fibrillary Acidic Protein (GFAP) 1:500 (Neuromics Antibodies, Edina, MN) for detection of astrocytes, anti Neurofilament 200 (NF200) 1:150 (Sigma Aldrich, Inc, Argentina) for neurons, anti Sex determining Region Y-box 2 (Sox2) (AbCam, Inc, Cambridge, CA) 1:200 for neural stem cells, anti Oligodendrocyte transcription factor 2 (Olig2) (Millipore, Temecula, CA) for glial restricted progenitors and anti Cluster of Differentiation 68 (CD68) (AbCam, Inc, Cambridge, CA) 1:100 for microglia and macrophages. After washing in PBS, sections were incubated with the appropriated secondary antibodies in the presence of 5 μM Höechst 33258 for nuclear staining. Secondary antibodies anti rabbit, anti mouse or anti chicken were purchased from Jackson Immunoresearch and were used in a 1:500 dilution. Finally, sections were washed in PBS, dried on glass slides and mounted in Mowiol® 4–88 mounting media.

Image analysis

Digital images were acquired with an epi-fluorescence microscope Olympus BX50, equipped with a CoolSnap digital camera. Quantitative analysis was performed with the Image ProPlus software. For MBP expression analysis, rectangular cortical sections (620 μm × 155 μm) were selected and processed as described in Suppl. Fig. 1. The distance

between pial surface and MBP$^+$ myelinated fibers edge was determined in each animal. Media from 6 to 10 animals of each experimental group were used to analyze differences between conditions. The same analysis was performed in 21 days old animals to confirm cortical layers were already myelinated before starting cuprizone intoxication. MBP positive area was also evaluated in these rectangular sections. Pixels having intensity values within a selected range were considered as MBP positive and area measurement was determined for each animal. Media for the different conditions were compared. For CC1 quantification, immunopositive cells were counted in square areas of interest (AOI) in both C_{35} and D_{35} brains (n = 5 for each condition). Similarly, for GFAP evaluation, positive cells were counted in square AOI including external cortical layers I–IV or internal VI layer next to subcortical white matter (n = 5 for each condition). Sox2$^+$ and Olig2$^+$ cells were counted in rectangular AOI selected inside cortical layers II–III and expressed as a percentage respect to total nuclei (n = 5 for each condition). Quantification of CAII$^+$ cells was performed by determining the percentage of CAII$^{+\,high}$ or CAII$^{+\,low}$ expressing cells in rectangular AOI located in cortical layers II–III (n = 5 for each condition). G ratio was calculated as the relation between the inner axonal diameter and total outer fiber diameter determined from electron microscopy cortical images (n = 3 for each condition).

Statistical analysis

Statistical analysis was performed using Student t-Test or one-way analysis of variance (ANOVA) followed by the Newman–Keuls post test (GraphPad Prism, GraphPad Software Inc., La Jolla, CA, USA). All data are given as means + SD. *P* values of the different analysis are given in the figure legends. Results were considered significant at *p* values less than 0.05.

Ultrastructural analysis

For Electron Microscopy (EM), three animals from each condition were killed by decapitation and brains were removed. A rectangular tissue block including the CC and a wedge-shaped section of the brain cortex were carefully excised as detailed in Suppl. Fig. 2 and fixed in a 2.5% glutaraldehyde in 0.1 M phosphate buffer. After rinsing in PBS, tissue blocks were postfixed in 1% osmium tetroxide in 0.1 M phosphate buffer, and then incubated in 5% uranile acetate. Specimens were dehydrated in ethanol at increasing concentrations (50, 75, 80 and 100%) and finally were embedded in araldite (Fluka Durcupan, Electron Microscopy Sciences) and polymerized for 3 days at 60 °C. Blocks were cut in 0.5 μm sections with an ultramicrotome (Ultracut E Reichert Jung) using glass knives. These semi-thin sections were stained with Toluidine Blue and observed with the optical microscope to confirm tissue preservation and sample orientation. Cortical tissue blocks were worn out 300 μm from the pial surface to reach cortical layers II–III. Finally, 70 to 90 nanometers ultra-thin sections were cut with the ultramicrotome and placed in copper grids (300 mesh number) and contrasted with lead citrate. Samples from the CC and cortex of each condition were observed with a transmission electron microscope EM109 Zeiss and photographed with a digital camera.

Results

Cuprizone effect on cortical detection of MBP

To study CPZ effects in rat brain cortex we used the intoxication protocol schematized in Fig. 1. Cortical myelin was evaluated by MBP immunohistochemical detection. As depicted in Figs. 2A and B, parietal cortex analysis was performed by identification of the different cortical layers I–V. We first show descriptive results that indicate MBP immunostaining was detected following the normal pattern of cortical axonal projections distributed throughout different layers in 35-day old rats (C_{35}) (Fig. 2C). Cuprizone treatment resulted in a marked demyelination of cortical layers I–III and part of layer IV in 35 day old animals (D_{35}) compared to controls (C_{35}) (Fig. 2D). For quantitative analysis, the distance between pial surface and the edge of myelinated fibers was measured to evaluate the extent of demyelination (see Materials and methods and Suppl. Fig. 1). Cuprizone intoxication generated a large area of subpial demyelination. We observed MBP depletion in a stripe 300 μm wide, including cortical layers I–III and part of layer IV in D_{35} animals (Fig. 2G, D_{35} vs C_{35}).

Effect of thyroid hormones during cortical remyelination

Demyelinated animals (D_{35}) were allowed to remyelinate in the absence of CPZ in the diet for an additional week, from P35 to P42 (Fig. 1). The quantitative analysis of the distance of the MBP$^+$ fibers from the pial surface showed a spontaneous remyelination process that took place in CPZ-treated animals between 35 and 42 days of age (Fig. 2G, D_{35} vs D_{35}–SS_{42}). We next tested whether the remyelination process could be enhanced by T3 treatment in the cortex, as was previously demonstrated for the CC, under this same intoxication protocol. To study TH effects on myelin recovery after demyelination, we decided to deliver T3 by intranasal instillation as an alternative and non-invasive administration route. The effects of T3 were evaluated by MBP immunohistochemical detection at 42 days of age (D_{35}–$T3_{42}$) and compared to saline treated controls (D_{35}–SS_{42}). Comparison of serum T3 levels at 2 h after intranasal or subcutaneous T3 administration revealed similar values (not shown) indicating that intranasal T3 rapidly crossed the nasal cavity epithelium and directly entered the blood stream. Descriptive immunohistochemistry images show that T3 treatment improved the cortical remyelination process compared to the SS treatment, as revealed by reappearance of MBP expression patterns in most external cortical layers (Figs. 2E, F). The T3 treated animals (D_{35}–$T3_{42}$) were less demyelinated than saline treated ones (D_{35}–SS_{42}) (Fig. 2G). Myelinated fibers of D_{35}–$T3_{42}$ rats reached similar distances from pia as animals which were never exposed to CPZ (Fig. 2G

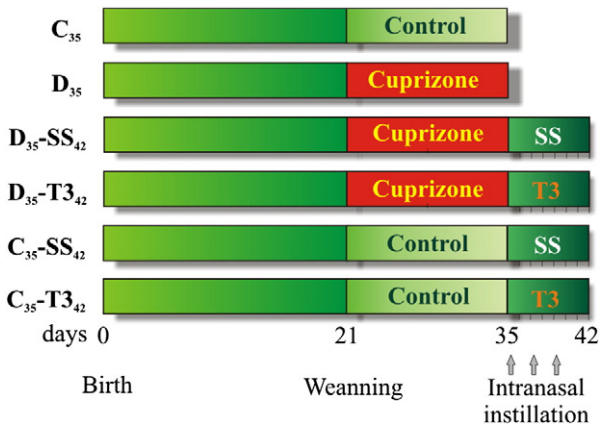

Fig. 1. Schematic representation of the CPZ intoxication protocol. Design of the different experimental conditions used in this study. Numbers at the bottom represent age of the animals (0, 21, 35 and 42 days). After weaning at 21 days of age, the rats were fed with milled chow pellet as a control diet (light green boxes between days 21 and 35) or supplemented with 0.6% CPZ for demyelination induction (red boxes between days 21 and 35). A group of animals was sacrificed at 35 days of age (control: C_{35} and demyelinated: D_{35}). Another group of control and demyelinated animals were maintained under a CPZ-free pellet chow diet for an additional week, from day 35 until day 42. During this remyelination period, animals were intranasally treated at 35, 37 and 39 days of age with SS (D_{35}–SS_{42} and C_{35}–SS_{42}) or T3 (D_{35}–$T3_{42}$ and C_{35}–$T3_{42}$) (arrows). These animals were sacrificed at 42 days of age. Animal nomenclatures indicate whether: a) animals were fed with control diet (C_{35}) or demyelinated by cuprizone (D_{35}), and b) the treatment used during remyelination period (SS_{42} or $T3_{42}$). C, control; D, demyelinated; SS, Saline Solution; T3, Thyroid hormone.

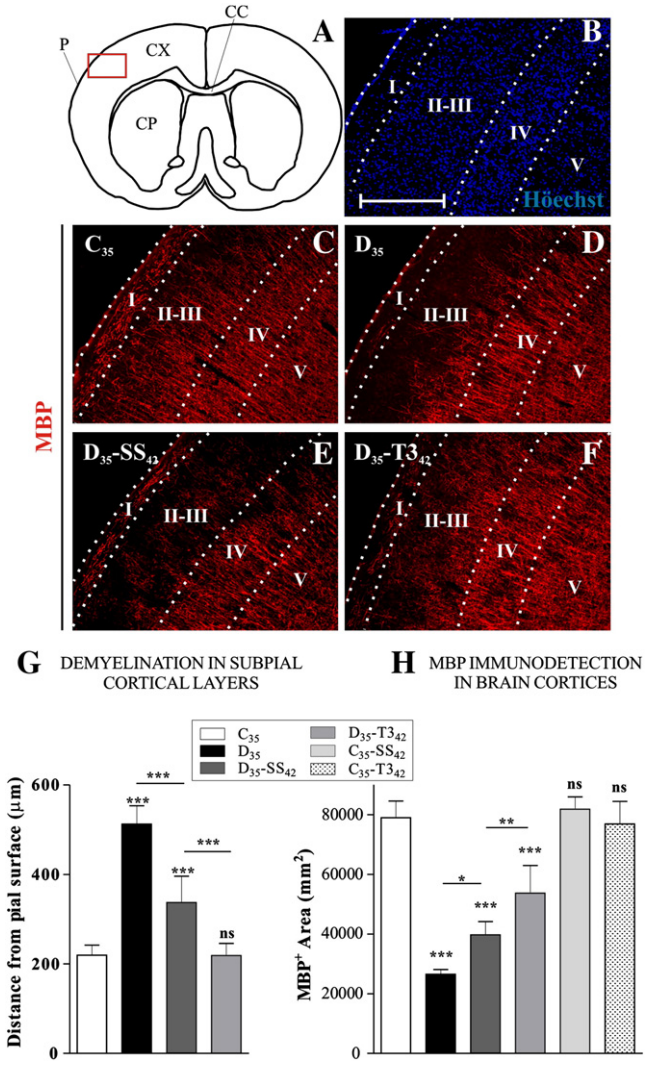

Fig. 2. Cuprizone administration induces demyelination in the rat brain neocortex. (A) Graphic representation of the selected cortical area for analysis. Outlined in red is the primary somato-sensory cortex. (B) Nuclei distribution in the cortex by Höechst 33258 staining. (C–F) IHC for MBP reveals the presence of myelinated tracts in the cortex with a radial distribution. (C–D) Control (C_{35}) and cuprizone-demyelinated (D_{35}) animals at 35 days of age showing demyelination in cortical layers I–III. (E–F) Cortical remyelination was evaluated 1 week after CPZ removal from the diet, at 42 days of age in animals receiving intranasal SS treatment (D_{35}–SS_{42}), or T3 treatment (D_{35}–$T3_{42}$). The boundaries between cortical layers I to V are indicated with white dashed lines (B–F). (G) Quantitative analysis of demyelination was performed by determining the length of MBP depletion measured from pial surface as described in Suppl. Fig. 1. The area of MBP^+ expression was also measured in similar sections from each condition using ImagePro Plus 5.1 software (H). T3 and SS treatments were also performed in control animals which were not exposed to CPZ (C_{35}–$T3_{42}$ and C_{35}–SS_{42}). Data sets for analysis were obtained from six to ten rats per group and were expressed as mean + SD. Data was analyzed by One way ANOVA followed by a Newman–Keuls post test. Statistical significance is indicated with asterisks over each bar and represents comparisons to C_{35}. Significances amongst different conditions are also indicated; $^*p \leq 0.05$, $^{**}p \leq 0.01$, $^{***}p \leq 0.001$, ns = not significant. Scale bar in B represents 200 µm for images B–F. I, II–III, IV and V represent brain neocortical layers; CC, Corpus callosum; CP, Caudate putamen; CPZ, Cuprizone; CX, Cortex; IHC, Immunohistochemistry; MBP, Myelin Basic Protein; P, Pial surface; and SS, Saline solution.

and Suppl. Fig. 1). The same quantitation strategy between control animals treated with SS (C_{35}–SS_{42}) or T3 (C_{35}–$T3_{42}$) did not show significant differences compared to C_{35} animals (not shown). Although MBP^+ fibers in D_{35}–$T3_{42}$ rats reached similar distances from the pial surface as C_{35} animals, the fluorescence density in the former seemed lower. We therefore decided to evaluate the myelin status by measuring MBP^+ pixel area as described in material and methods section (Fig. 2H). We found that MBP expression was reduced by 60% in demyelinated rats (D_{35}) compared to controls (C_{35}). MBP immunoreactivity was partially recovered in 42-day old animals undergoing spontaneous remyelination (D_{35}–SS_{42}). Although T3 treated animals (D_{35}–$T3_{42}$) did not fully restore normal myelin levels, MBP expression was significantly higher compared to saline treated animals (D_{35}–SS_{42}). MBP expression levels of C_{35}–SS_{42} and C_{35}–$T3_{42}$ were undistinguishable from those found in 35 days old control rats (C_{35}) (Fig. 2H). Taken together, these results confirmed that cortical demyelination takes place in rat brain during CPZ intoxication and that remyelination process in the cortex is regulated by T3 hormone.

Oligodendrocyte loss in the cortex after cuprizone intoxication

Since MBP is mainly expressed in OL processes, we studied whether loss of MBP immunostaining in the cortex was a consequence of OL process retraction or directly correlates with oligodendroglial cell loss. Immunohistochemical analysis using CC1 antibody, which predominantly labels mature OL cell bodies, showed a 65% reduction in the percentage of positive cells in D_{35} animals compared to same age controls (Figs. 3A–E). These results suggest that lack of MBP expression in the cortex of CPZ-intoxicated rats was a consequence of a reduction in the number of cortical OL. $NF200^+$ nude axons were detected in the cortex of D_{35} animals, indicating that neuronal tracts are still present in these demyelinated areas (Fig. 3F).

The observation of MBP immunostaining in other brain regions showed that CPZ-induced demyelination was not restricted to the somato-sensory cortex. Motor cortex and cingulated cortex were affected as well (Figs. 4A, B). Furthermore, cortices of CPZ-intoxicated rats were similarly affected at different rostro-caudal positions (not shown). In the septum, MBP immunostaining was also reduced (Figs. 4C, D). Immunodetection of MBP in the caudate putamen (Figs. 4F, G) showed less appreciable differences between C_{35} and D_{35} rats.

Cuprizone-induced astrogliosis in the brain cortex

Astroglial distribution was evaluated by immunohistochemistry against GFAP. Astrocyte proportions were duplicated in D_{35} compared to C_{35}, both in most superficial cortical layers (I–IV) (Figs. 5A, B, I) as in deeper layers (VI) (Figs. 5E, F, J). Despite MBP recovery during remyelination, astrogliosis persisted in both D_{35}–SS_{42} and D_{35}–$T3_{42}$ animals when compared to non-demyelinated control animals (Figs. 5C, D, G, H, I, J). However, even though astrocyte proportion did not reach control values, $GFAP^+$ cell numbers decreased in deeper cortical layers of D_{35}–$T3_{42}$ rats compared to D_{35}–SS_{42} (Figs. 5G–J). In D_{35} animals, MBP and GFAP double staining showed that higher levels of astrogliosis were observed near the areas displaying depletion of MBP expression in CPZ animals (Figs. 6A and B).

Marker characterization in the cortex after demyelination and remyelination

We analyzed the expression patterns of Sox2 and Olig2, two transcription factors associated with undifferentiated neural stem cells and glial restricted progenitor cells, respectively. In C_{35} rats, both nuclear factors seem to be expressed by cells homogeneously distributed throughout the cortex (Fig. 6C). Most of these cells expressed either Sox2 or Olig2, however we were able to detect a few cells displaying co-localization of both factors. We detected a 75% increase in the numbers of $Sox2^+$ cells (Figs. 6C, D, G) and 50% increase in the numbers of $Olig2^+$ glial progenitors (Figs. 6C, D, H) in D_{35} animals, compared to controls. Both Sox2 and Olig2 were mainly up-regulated in layers II–III, where demyelination is more pronounced (Fig. 6D). During remyelination, T3 treatment (D_{35}–$T3_{42}$) normalized Sox2 and Olig2 cell numbers to the control values, while in saline controls (D_{35}–SS_{42}), activation of $Sox2^+$ cells still persisted (Figs. 6 G, H). The expression of the microglia/macrophage marker CD68 was not detected in the

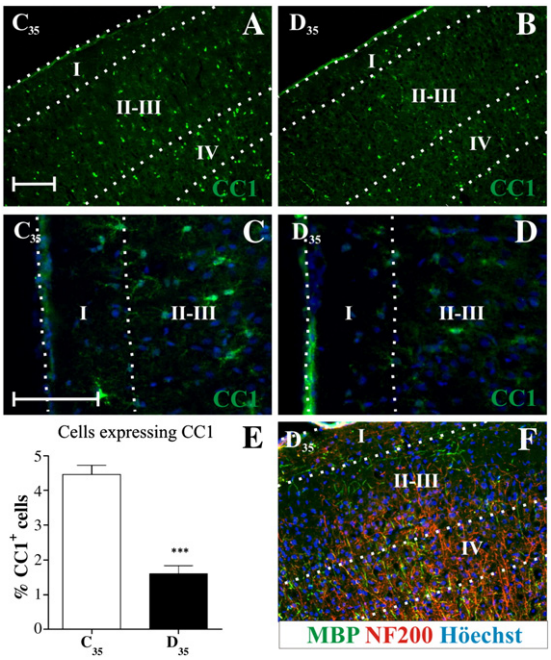

Fig. 3. Oligodendrocyte loss after CPZ intoxication. (A–D) IHC analysis for the mature OL marker CC1 shows the decrease in the number of cortical OLs in CPZ intoxicated rats (D_{35}) compared to controls (C_{35}) at 35 days of age. C–D show higher magnification images of cortical layers I, II–III. For quantitative analysis, data are expressed as media + SD of the percentage of $CC1^+$ cells respect to total nuclei from identical AOI, and statistical analysis was performed using the Student's t Test (***$p \leq 0.001$, $n = 5$) (E). Double immunostaining for MBP (green) and neuronal marker NF200 (red) showed that nude neuronal fibers are still present in demyelinated cortical areas of C_{35} animals. Nuclei are in blue by Höechst staining (C, D, F). Dotted lines indicate the boundaries between neocortical brain layers (I to IV). Scale bar in A represents 100 μm for A, B and F and scale bar in C equals 100 μm for C and D. CC1, anti Adenomatous Poliposis Coli monoclonal antibody clone 1; CPZ, Cuprizone; IHC, Immunohistochemistry; MBP, Myelin Basic Protein; NF200, Neurofilament 200; OL, Oligodendrocyte; and AOI, area of interest.

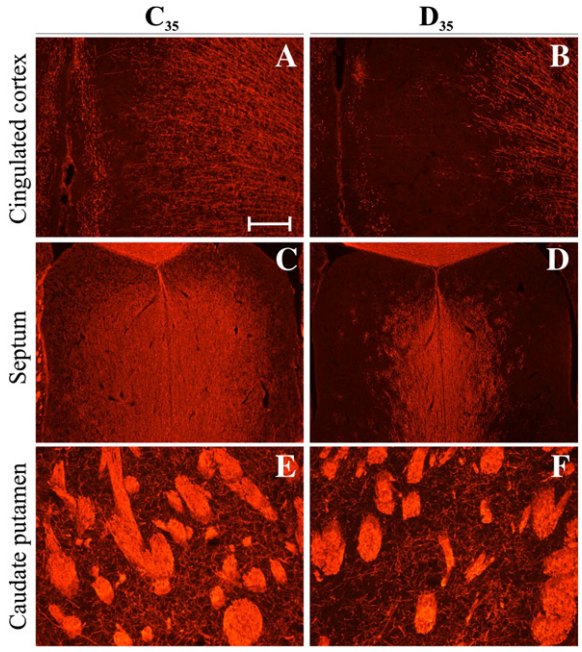

Fig. 4. Cuprizone effects on different brain regions. IHC for MBP showing staining reduction in demyelinated animals (D_{35}) respect to same age controls (C_{35}) in the cingulated cortex (A–B) and the septum (C–D). Areas with higher myelin content, as the caudate putamen, were less affected (E–F). Scale bar in A represents 100 μm. IHC, immunohistochemistry.

cortex of control brains (Fig. 6I) and rarely detected in CPZ-intoxicated rats (Fig. 6J, arrowhead), suggesting microglial activation is not a relevant process during cortical demyelination. CAII expression was also studied, as it covers all stages of the oligodendroglial lineage. We found an increase in the numbers of $CAII^+$ cells in cortical layers II to IV of D_{35} animals (Figs. 6I, J). The observation that both OL markers MBP and CC1 were depleted in these cortical areas, lead us to investigate the identity of these $CAII^+$ activated cells. We analyzed co-location patterns for CAII and CC1 in each condition (Fig. 7). Control brains showed that almost all $CAII^+$ cells were also $CC1^+$, indicating they were mature OL (Figs. 7A, E, I, arrowhead). We were able to detect a few $CAII^+/CC1^-$ and $CAII^-/CC1^+$ cells in C_{35} rats (Fig. 7I). On the contrary, cortical $CAII^+$ cells in D_{35} brains were $CC1^-$, suggesting they were not mature OL (Figs. 7B, F, J). Furthermore, while CAII expression in C_{35} was strong and mostly restricted to $CC1^+$ OL soma (named $CAII^{+high}$) (Fig. 7A), $CAII^+$ cells in D_{35} brain cortex displayed a remarkably lower CAII expression in star shaped cells (Fig. 7B) (named $CAII^{+low}$). This particular morphology of $CAII^{+low}$ cells in the cortex of D_{35} animals is not reproduced in the CC, where $CAII^+$ cells conserved typical OL morphology ($CAII^{+high}$) and co-localized with CC1 (not shown). We next studied CAII pattern expression in brains undergoing remyelination. Both D_{35}–SS_{42} and D_{35}–$T3_{42}$ animals showed the presence of some $CAII^+/CC1^+$ OL ($CAII^{+high}$), although $CAII^+/CC1^-$ star-shaped cells ($CAII^{+low}$) were still observed (Figs. 7C, D, G, H, K, L). Because CAII was previously found to be expressed in astrocytes during early development and some pathological conditions, we studied whether $CAII^+$ cells in D_{35} rats could belong to the astroglial lineage. Double immunodetection showed cortical $CAII^{+low}$ cells overlapped with GFAP immunostaining (Figs. 7N, R), indicating they were actually astrocytes. The increase in the numbers of $CAII^{+low}$ cells was observed in cortical layers III–IV of CPZ animals, where maximal astrogliosis was detected (Fig. 7N). In the cortex of C_{35} animals, $CAII^+$ OL with immuno-positive rounded soma (Figs. 7M, Q, filled arrowhead) clearly differentiated from $GFAP^+$ astrocytes (Figs. 7M, Q, open arrowheads). Contrarily, in D_{35} animals, cortical OL with this classical morphology ($CAII^{+high}$) were lost (Fig. 7R). Instead, CAII was expressed in a more diffuse way in $GFAP^+$ astrocytes ($CAII^{+low}$) (Fig. 7R, arrow). Animals undergoing remyelination showed re-expression of CAII in cells with typical oligodendroglial morphology ($CAII^{+high}$) (Figs. 7O, P, S, T). Higher magnification images showed the presence of $CAII^{+high}$ OL (filled arrowhead in Figs. 7S, T) clearly distinguished from $GFAP^+$ astrocytes (empty arrowhead in Figs. 7S, T). However, we still observed some $GFAP^+$ astrocytes co-expressing CAII ($CAII^{+low}$) in both D_{35}–SS_{42} and D_{35}–$T3_{42}$ animals (arrow in Figs. 7S, T). Quantification of $CAII^+$ cells in each condition (Figs. 7U, V) confirmed that $CAII^{+high}$ oligodendrocytes were markedly reduced in D_{35} rats and were recovered during remyelination (Fig. 7U). Contrarily, $CAII^{+low}$ reactive astrocytes were upregulated in D_{35} animals and reach normal numbers during remyelination (Fig. 7V).

Myelin analysis by electronic microscopy

Ultrastructural analysis was performed to compare cortical and CC demyelination by CPZ intoxication as well as to evaluate remyelination process after T3 treatment (Fig. 8). Electron microscopy analysis was performed on CC and brain cortex samples as depicted in Suppl. Fig. 2. Myelin sheaths of the CC were not severely affected in D_{35} rats compared to same age controls (Figs. 8A and B). Contrarily to CC findings, myelinated axons in the cortex were markedly affected after two weeks of CPZ intoxication (Figs. 8G, H). Notwithstanding, general tissue organization was preserved in the cortex of D_{35} animals, we found a severe reduction in the thickness of myelin sheaths compared to controls (Figs. 8M, N). Although CPZ intoxication was ended at 35 days of age, severe demyelination of CC axons was later detected at 42 days of age, a week after CPZ removal from the diet (Fig. 8C). Trans-callosal axonal projections were markedly demyelinated in

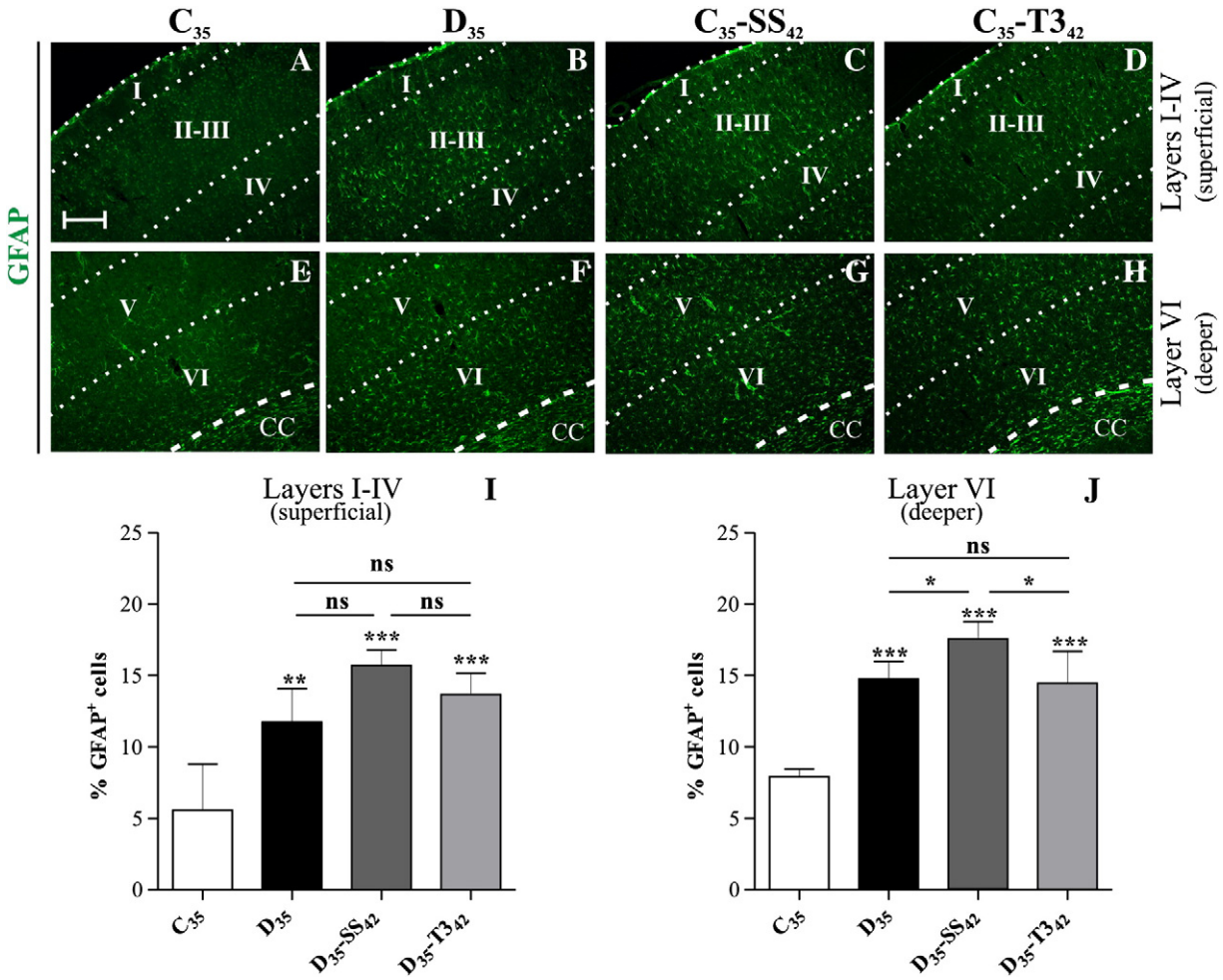

Fig. 5. Cortical astrogliosis during demyelination and remyelination. IHC for GFAP in cortical areas of animals under different experimental conditions. Most superficial cortical layers I to IV (close to pia) are shown in A–D. The deeper cortical layer VI is adjacent to the CC and was analyzed in E–H. For quantitation, identical AOI were selected next to pial surface (for A–D) or next to the CC (E–H) and percentage of GFAP positive astrocytes were normalized to the total nuclei, as shown in I (layers I–IV) and J (layer VI). Data was expressed as media + SD. Analysis was performed by One way ANOVA followed by the Newman–Keuls post test. Statistical significance is indicated with asterisks over each bar and represents comparisons to C_{35}. Significances amongst different conditions are also indicated; * $p \leq 0.05$, ** $p \leq 0.01$, *** $p \leq 0.001$, ns = not significant. Dotted lines indicate boundaries between cortical layers and the dashed line limits gray matter and the CC subcortical white matter. Scale bar in A equals 100 μm for all images. AOI, Area of Interest; CC, Corpus callosum; GFAP, Glial Fibrillary Acidic Protein; IHC, Immunohistochemistry; I, II–III, IV and V represent brain neocortical layers.

D_{35}–SS_{42} rats (Fig. 8C) compared to C_{35}–SS_{42} (Fig. 8E). Loss of tissue integrity was one of the most remarkable findings both in the CC (Fig. 8C) as well as in the cortex (Fig. 8I) of CPZ animals at 42 days of age. Majority of cortical axons displayed disrupted myelin sheaths with splits between lamellae and brain parenquima seem to be strongly affected when compared to same age controls (Figs. 8I, K, O, Q). Comparison between D_{35}–SS_{42} and D_{35}–$T3_{42}$ rats revealed a higher recovery of myelin thickness in the CC in T3 treated CPZ animals compared to controls (Figs. 8C, D, S). Myelinated axons were also restored in the cortex of D_{35}–$T3_{42}$ animals when compared to D_{35}–SS_{42} (Figs. 8I, J, S), although some myelin disarrangement was still observed in both conditions (Figs. 8I, J, O, P). Corpus callosum and cortical myelin sheaths from control animals treated with T3 were indistinguishable from saline treated controls (C_{35}–$T3_{42}$ and C_{35}–SS_{42}) (Figs. 8E, F, K, L, Q, R, S). Representative higher magnification images of individual cortical axons confirmed myelin ultrastructural changes observed in these animals (Figs. 8M–R). For quantification, we analyzed G ratio from each experimental condition (Fig. 8S). Cuprizone intoxication affected myelin thickness in the brain cortex of D_{35} rats. During remyelination, T3 administration was shown to improve myelin restoration in the cortex with respect to saline treatment. All together, our results indicate that the CPZ effect on the cortex is an early event that precedes CC demyelination. Furthermore, T3 is able to partially restore myelin sheath structures in the cortical region.

Discussion

Cortical demyelination and neuronal degeneration are common findings in postmortem MS brains (Bo et al., 2003b; Kutzelnigg and Lassmann, 2005; Kutzelnigg and Lassmann, 2005, 2007; Peterson et al., 2001). Mechanisms of demyelination in the cortex have generated great interest in the last few years, as it seems to occur without participation of microglia or immune cells from blood, both being prominent features of white matter demyelination (Albert et al., 2007; Kutzelnigg et al., 2005; Peterson et al., 2001). Most studies in animal models have evaluated demyelination in white matter enriched structures of the brain, such as the CC and cerebellar peduncles (Blakemore, 1973, 1974; Matsushima and Morell, 2001). However, several groups have recently described cortical demyelination both in CPZ-intoxicated mice (Gudi et al., 2009; Silvestroff et al., 2010; Skripuletz et al., 2008) as well as in EAE-induced mice (Girolamo et al., 2011; Mangiardi et al., 2011). Here we show that CPZ-intoxicated rats display demyelination in the brain cortex, which resembles type III lesions found in progressive MS patients (Dutta and Trapp, 2011; Peterson et al., 2001). Immunodetection of MBP at the end of the

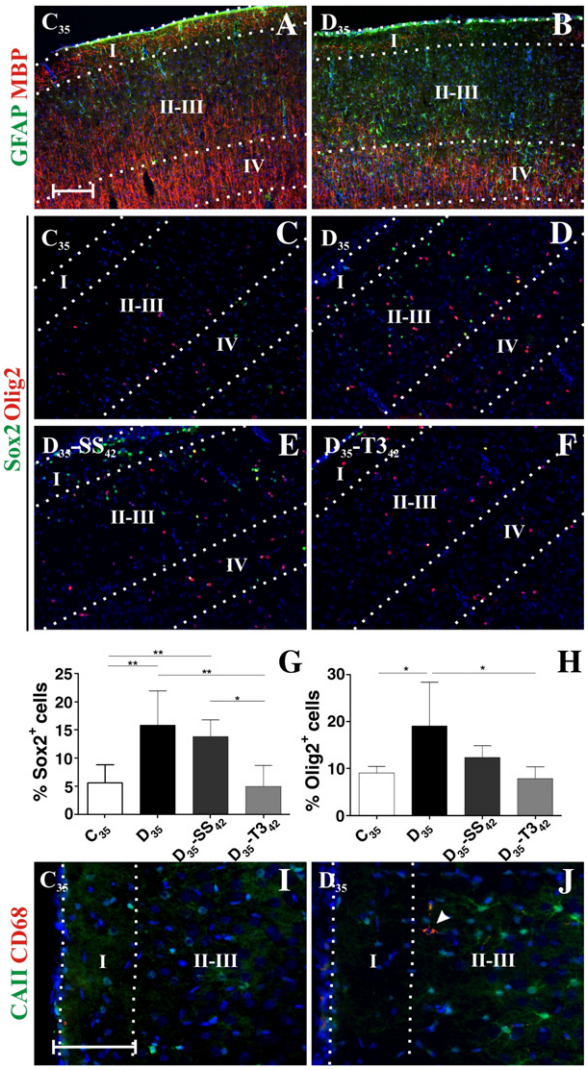

Fig. 6. Immunohistochemical characterization during cortical demyelination and remyelination. Double IHC for MBP (red) and GFAP (green) in superficial cortical layers showing that MBP depleted areas in D_{35} animals correlate with astrogliosis around the boundary between layers II–III and IV (A, B). Sox2 and Olig2 are expressed in neural stem cells and glial restricted progenitor cells, respectively, in the cortex of C_{35} rats (C). After CPZ-induced demyelination (D_{35}), the numbers of $Sox2^+$ and $Olig2^+$ cells increased in cortical layers II–III (D, G, H). Activation in the expression of Sox2 and Olig2 is still detected in D_{35}–SS_{42} animals (E, G, H). T3 treatment during remyelination restores $Sox2^+$ and $Olig2^+$ cell numbers to those found in control animals (F, G, H). Quantification of both markers is shown in G and H. Data are expressed as the percentage of positive cells with respect to total nuclei in selected areas included in layers II–III. Analysis was performed by One way ANOVA followed by the Newman–Keuls post test and significances between conditions are indicated $^*p \leq 0.05$, $^{**}p \leq 0.01$, $^{***}p \leq 0.001$. Double IHC for CAII (green), which labels all stages of the oligodendroglial lineage and CD68 (red), a microglia/macrophage marker is shown in I and J, and nuclei are stained in blue. CAII expression was up-regulated in the cortex of D_{35} rats compared to C_{35} (for quantification see Fig. 7). CD68 was not detected in superficial cortical layers of C_{35} rats (I) and rarely detected in D_{35} (arrowhead in J). Scale bar in A represents 200 μm for A–F and 100 μm for I–J. Dotted lines indicate the boundaries between cortical layers. CAII, Carbonic Anhydrase isoform II, CD68, Cluster of Differentiation 68; GFAP, Glial Fibrillary Acidic Protein; IHC, Immunohistochemistry; MBP, Myelin Basic Protein; I, II–III, IV and V represent brain neocortical layers.

intoxication period revealed areas of subpial demyelination throughout the cortex, including somato-sensory and motor cortex at different rostro-caudal positions. We demonstrated that lack of MBP^+ myelin is due to a reduction in the number of $CC1^+$ OL. These results are in agreement with those recently found in the EAE mouse model (Girolamo et al., 2011; Mangiardi et al., 2011). Furthermore, demyelinated cortical layers showed the presence of $NF200^+$ nude axons. Although this does not confirm axonal indemnity, it strongly suggests that OL are the most CPZ-susceptible cell type in the cortex.

As previously demonstrated in the mouse CPZ model (Skripuletz et al., 2008), we found that demyelination in the cortex was detected earlier than in white matter-enriched structures. Initial studies from our laboratory using this same intoxication protocol in rats showed severe demyelination in the CC at 35 days of age (Adamo et al., 2006). In the present work, ultrastructural analysis indicates that the CC was not as severely affected in D_{35} brains. This apparent discrepancy could be explained by the brain sections analyzed in each study. In the present study, brains were analyzed at a more rostral level (+1.4/−0.3 mm from bregma), while in previous work we have described supra-hippocampal white matter changes at more caudal positions (−2.3 mm from bregma). In fact, it has been shown that CPZ-induced demyelination produces a dramatic rostro-caudal gradient of white matter demyelination, being caudal CC more injured than rostral area (Wu et al., 2008; Xie et al., 2010). Nevertheless, at 42 days of age, both the cortex and the CC were intensely demyelinated as detected by immunofluorescence of specific markers as well as by ultrastructural analysis. Furthermore, myelin loss in D_{35}–SS_{42} animals was also accompanied by severe tissue disorganization in both brain structures.

It is well established that THs are required for oligodendrogenesis and myelin formation during development (Baas et al., 1997; Barres et al., 1994; Baumann and Pham-Dinh, 2001; Bhat et al., 1979; Billon et al., 2001; Fernandez et al., 2004b; Marta et al., 1998; Pasquini and Adamo, 1994; Rodríguez-Peña, 1999). Although TH was shown to promote remyelination in white matter structures (Fernandez et al., 2004a; Franco et al., 2008), to this date no studies have described TH effects on cortical brain tissue.

Intranasal administration is considered an alternative pathway for drug delivery to the CNS that by-passes the BBB (Illum, 2000). This strategy has not only been used in the basic research field (Alcalá-Barraza et al., 2010; Cai et al., 2011; Scranton et al., 2011; Thorne et al., 2004), but has found concrete applications in human health (Jogani et al., 2008; Pathan et al., 2009). There is some disbelief whether there exists an efficient transport of molecules directly to the CNS through the ethmoides cribiform plate, either vía the perineural space or by direct olfactory axon transport (Merkus and van den Berg, 2007), or whether drugs cross the nasal epithelium to systemic blood circulation before reaching the CNS. Nonetheless, in this particular work we disregard the mechanisms of entry of TH to the CNS. Even if there is no direct transport to the CNS through the olfactory bulb, THs are able to cross the BBB.

In this work, we performed intranasal delivery of T3 in CPZ-demyelinated rats and analyzed progression of remyelination process in comparison to saline treated siblings. We found that T3 rapidly disseminates into blood stream, preventing restriction to the CNS. Several trans-membrane transporters mediate TH uptake from blood into brain (Kinne et al., 2011). Particulary, MCT8 is highly expressed in endothelial cells of cerebral microvessels and is able to transport T3 across the BBB into brain parenchyma (Friesema et al., 2003; Kinne et al., 2011; Roberts et al., 2008).

Similarly to what was previously described for white matter enriched structures (Franco et al., 2008), T3 promotes a significant improvement in cortical myelin recovery when compared to saline treated animals. Thereafter, mechanisms of T3 action on remyelination seem to be conserved between white and gray matter.

We found that the microglia/macrophage marker CD68 was not activated in most external cortical layers of D_{35} rats, in which demyelination was more prominent. This result indicates that these particular immune cells did not play a relevant role during cortical demyelination. It is also tempting to speculate that microglial activation directly correlates with myelin content of each brain structure. Our results are in accordance with previous findings that show only

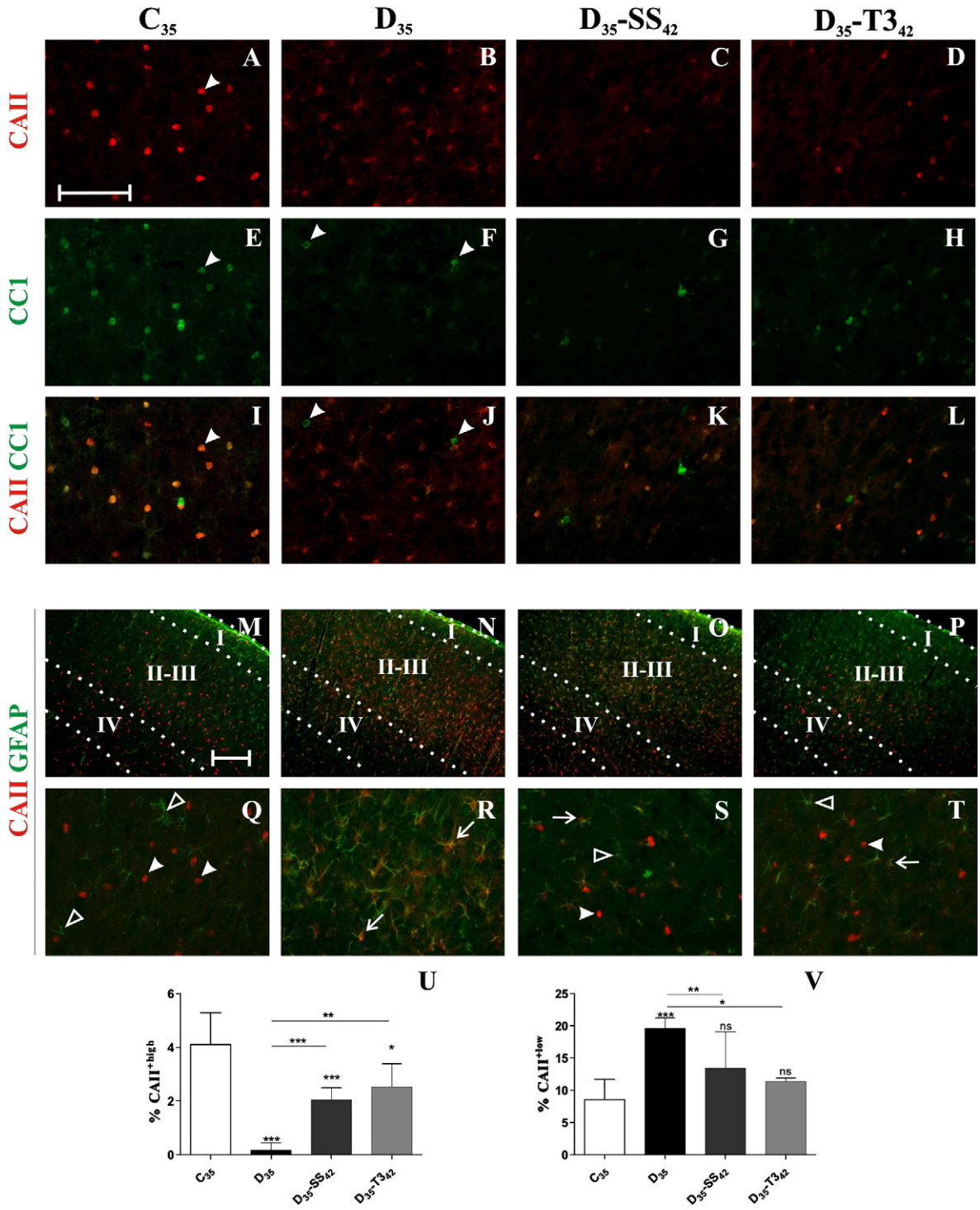

Fig. 7. CAII expression shifts from OLs to astrocytes during cortical demyelination. CAII expression was studied in cortical layers II–III in C_{35} (A) and CPZ-demyelinated D_{35} animals (B) at 35 days of age, and in remyelinating D_{35}–SS_{42} (C) and D_{35}–$T3_{42}$ (D) rats. Mature oligodendrocyte marker CC1 was analyzed in the same experimental conditions (E–H). Merged images of CAII and CC1 are shown in (I–L). Arrowheads in A, E and I show overlapping expression of CC1 and CAII in C_{35} animals. Arrowheads in F and J indicate $CC1^+$ OLs lacking CAII expression. Merged images of CAII (red) and GFAP (green) are shown in M–T. In C_{35} animals, CAII expression is restricted to the oligodendroglial lineage (I, Q). Contrarily, astrogliosis in cortical layers II–III of D_{35} animals overlaps to CAII (M, N). Higher magnification images from each experimental condition are shown in Q–T. Filled arrowheads point on $CAII^+$ OLs, open arrowheads indicate $GFAP^+$ astrocytes, and arrows mark $GFAP^+/CAII^+$ cells. For quantitative analysis, $CAII^+$ cells with higher expression levels ($CAII^{+\,high}$), corresponding to mature OL, were determined in rectangular AOI inside cortical layers II–III. Data is expressed as the percentage of $CAII^{+\,high}$ respect to total nuclei (U). Cells with low CAII expression ($CAII^{+\,low}$), corresponding to reactive astrocytes, were also quantified and expressed as the percentage respect to total nuclei (V). Analysis was performed by One way ANOVA followed by the Newman–Keuls post test and significances between conditions are indicated $^*p \leq 0.05$, $^{**}p \leq 0.01$, $^{***}p \leq 0.001$. Scale bar in A represents 200 μm for A–L and Q–T, and scale bar in M equals 200 μm for M–P. Dotted lines indicate boundaries between cortical layers I to IV. CAII, Carbonic Anhydrase isoform II; CC1, anti Adenomatous Poliposis Coli monoclonal antibody clone 1; GFAP, Glial Fibrillary Acidic Protein; and OL, Oligodendrocyte.

sporadic activated microglia in demyelinated animals, restricted to deeper cortical layers next to the CC and absent from most external ones (Gudi et al., 2009).

Astrogliosis has been extensively described in demyelinating models (Gudi et al., 2009; Norton et al., 1992; Skripuletz et al., 2008; Tani et al., 1996). We confirmed that numbers of $GFAP^+$ cells

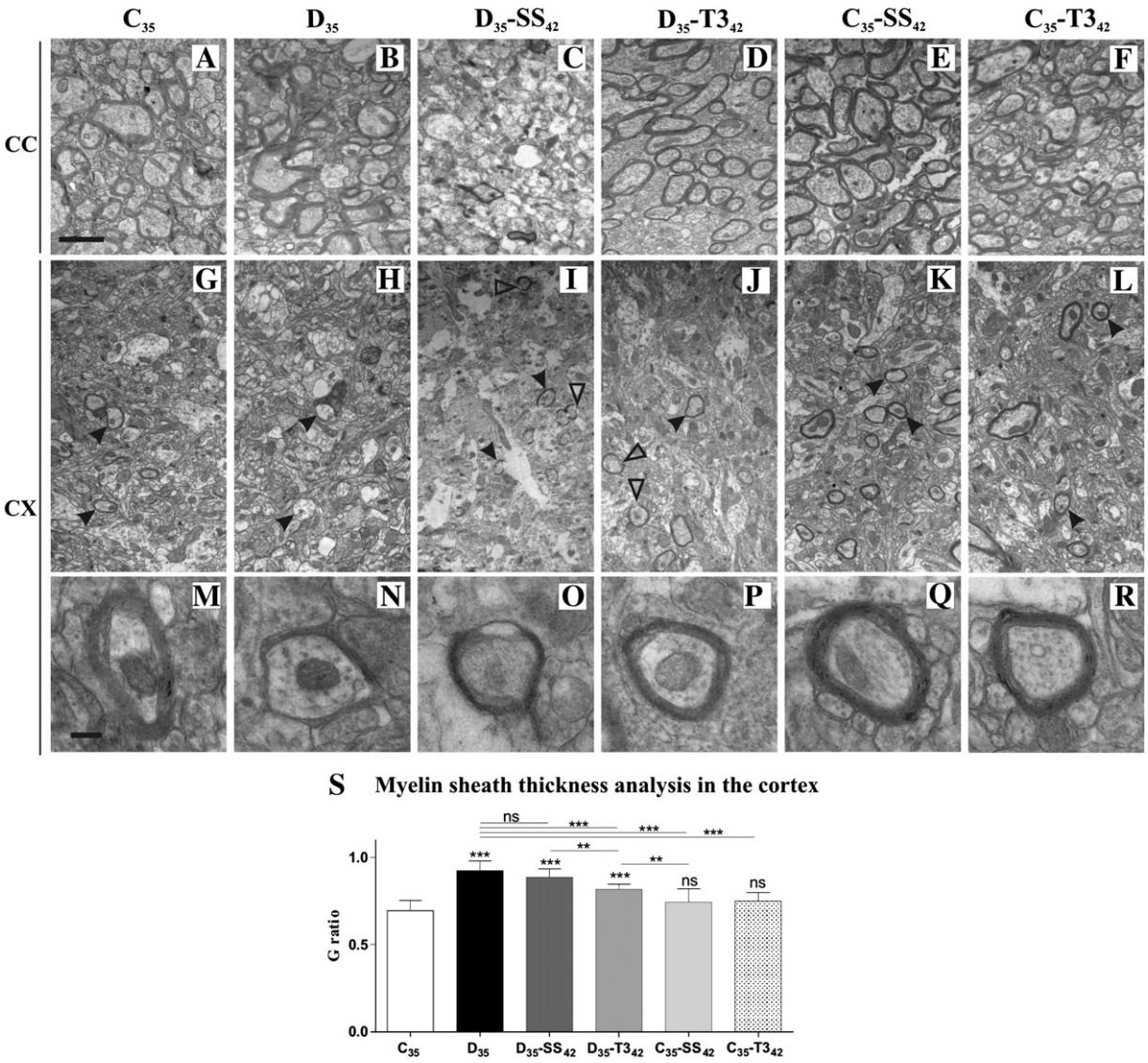

Fig. 8. Ultrastructural analysis during demyelination and remyelination. EM images of the CC in the different experimental conditions are shown in A–F. Similar analysis al the level of cortical layers II–III is shown in G–L. Higher magnification images of individual cortical axons are shown in M–R. For a detailed description of the areas under analysis, see Supplementary Fig. 2. Myelin sheaths in the CC of D_{35} rats, were morphologically similar to control animals (A, B). D_{35}–SS_{42} animals show myelin loss together with a general tissue disorganization (C). Myelin sheaths were partially recovered in the CC of T3 treated animals (D). SS or T3 treatments do not affect myelin structure when administered to control animals (E, F). In the brain cortex, myelin sheath thickness was markedly reduced in D_{35} rats (black arrowheads in H, N, S) when compared to control cortex (black arowheads in G, M, S). In D_{35}–SS_{42} rats (I, O, S) thickness of myelin sheaths is still reduced (black arowheads in I) and similarly to the CC, tissue disorganization is also prominent in the cortex. Several axons show structural alterations in their myelin sheaths (open arrowheads in I). In D_{35}–$T3_{42}$ cortices (J, P, S) despite the fact that partial recuperation in myelin thickness occurs, structural sheaths alterations still persist (open arrowheads in J). As well as in the CC, animals which were not exposed to CPZ, were not affected by SS (K, Q) and T3 (L, R) treatments (S). G ratio was calculated as the cocient between inner axonal diameter and total fiber diameter and plotted in S ($n = 3$ animals for each condition). Analysis was performed by One way ANOVA followed by the Newman–Keuls post test and significances between conditions are indicated $^{**}p \leq 0.01$, $^{***}p \leq 0.001$, ns, not significant. CC, Corpus callosum; CX, Cortex; SS, saline solution; CPZ, cuprizone, and EM, Electron microscopy. Scale bar in A represents 2 μm for A to L. Scale bar in M equals 0.2 μm for M to R. Black arrowheads indicate myelinated cortical axons in G–L.

rise in the cortex of demyelinated rats in particular layers and coincide with MBP depleted cortical brain regions. One week after CPZ removal from the diet, astrogliosis still persists. Whether astrogliosis acts as a desmyelinating effector and/or if it plays a major role during remyelination reparative process is not fully clarified.

We found an increase in the numbers of $Sox2^+$ neural stem cells and $Olig2^+$ glial progenitors in layers II–III of CPZ rats, suggesting that endogenous response to CPZ-demyelination is predominated by new waves of oligodendrogenesis from local stem cells and glial restricted progenitors. Subpial cortical area has been characterized as an additional niche for oligodendrogenesis in developing murine brain (Costa et al., 2007). Reactivation of oligodendrogenesis in this region has been previously proposed in EAE mouse model (Girolamo et al., 2011). $Sox2^+$ activation persisted in D_{35}–SS_{42} animals, indicating remyelination process was fully progressing. Contrarily, in T3 treated rats (D_{35}–$T3_{42}$) both Sox2 and Olig2 cell numbers were returned to normal values, suggesting they were not needed anymore for the cortical repairment process.

We found a marked increase in the numbers of $CAII^+$ cells in the cortex of demyelinated animals compared to controls. Based on the accepted CAII expression in the OL of both white and gray matter of the adult brain, this finding seemed contradictory with the reduction in the numbers of $CC1^+$ OL registered in CPZ brains. Further analysis revealed that $CAII^+$ cells in the cortex of D_{35} animals morphologically resembled protoplasmic astrocytes and also expressed GFAP. Thus, our results indicate a shift in the localization of CAII from OL to astrocytes during CPZ feeding. This coincides with data describing CAII expression in reactive astrocytes during gliosis as well as other markers such as glutation-S-transferase Pi isoform, Nestin, RC1,

BLBP and Vimentin in several injury models (Cammer and Zhang, 1993; Cammer et al., 1989; Gudi et al., 2009; Kipp et al., 2011; Talbott et al., 2005; Tamagno and Schiffer, 2006). During CNS development, CAII expression has been detected in glial precursor cells in the forebrain of neonatal rats, and is differentially expressed as cells differentiate, being down-regulated in astrocytes and up-regulated in OL (Cammer and Zhang, 1992). It is tempting to speculate that this compensatory mechanism recapitulates some aspects of postnatal CNS development. In particular, it has been shown that Nestin$^+$ reactive astrocytes do not proliferate and give rise to NG2$^+$ cells, suggesting an astrocytic de-differentiating process in an attempt to regenerate oligodendroglial population (Talbott et al., 2005).

Our results clearly demonstrated that striking demyelination takes place in the brain cortex of Wistar rats under CPZ intoxication which could serve as a useful model to study mechanisms of cortical pathology in MS. Taken together with previous data, the present work demonstrates that TH participates in the control of CNS repair mechanisms, both in white and gray matter. Evidence showing an increased prevalence of thyroid disorder in MS patients (Kiessling et al., 1980; Munteis et al., 2007; Niderwiesser et al., 2003) highlights the relevance of this hormonal pathway in the disease progression and suggests that TH treatment could be used as an effective therapeutic intervention in MS.

Supplementary materials related to this article can be found online at doi:10.1016/j.expneurol.2012.02.018.

Acknowledgments

The authors are grateful to M. J. Pérez for helpful comments on the manuscript and continuous support and Dr N. Sanjuan for technical assistance with electron microscopy. Grant sponsors: PIP 112-200801-01767 from CONICET to P.F., PICT 0791 from ANPCyT to J.P. and UBACYT 20020090200481 to P.F.

References

Adamo, A., Paez, P., Escobar Cabrera, O., Wolfson, M., Franco, P., Pasquini, J., Soto, E., 2006. Remyelination after cuprizone-induced demyelination in the rat is stimulated by apotransferrin. Exp. Neurol. 198, 519–529.
Albert, M., Antel, J., Brück, W., Stadelmann, C., 2007. Extensive cortical remyelination in patients with chronic multiple sclerosis. Brain Pathol 17, 129–138.
Alcalá-Barraza, S., Lee, M., Hanson, L., McDonald, A., Frey, W., McLoon, L., 2010. Intranasal delivery of neurotrophic factors BDNF, CNTF, EPO and NT-4 to the CNS. J. Drug Target. 18, 179–190.
Baas, D., Bourbeau, D., Sarlieve, L., Ittel, M., Dussault, J., Puymirat, J., 1997. Oligodendrocyte maturation and progenitor cell proliferation are independently regulated by thyroid hormone. Glia 19, 324–332.
Barres, B., Lazar, M., Raff, M., 1994. A novel role for thyroid hormone, glucocorticoids and retinoic acid in timing oligodendrocyte development. Development 120, 1097–1108.
Baumann, N., Pham-Dinh, D., 2001. Biology of oligodendrocyte and myelin in the mammalian central nervous system. Physiol. Rev. 81, 871–927.
Bhat, N., Sarlieve, L., Rao, G., Pieringer, R., 1979. Investigations on myelination in vitro: regulation by thyroid hormone in cultures of dissociated brain cells from embryonic mice. J. Biol. Chem. 254, 9342–9344.
Billon, N., Tokumoto, Y., Forrest, D., Raff, M., 2001. Role of thyroid hormone receptors in timing oligodendrocyte differentiation. Dev. Biol. 235, 110–120.
Blakemore, W., 1973. Remyelination of the superior cerebellar peduncle in the mouse following demyelination induced by feeding cuprizone. J. Neurol. Sci. 20, 73–83.
Blakemore, W., 1974. Pattern of remyelination in the CNS. Nature 249, 577–578.
Bo, L., Vedeler, C., Nyland, H., Trapp, B., Mork, S., 2003a. Intracortical multiple sclerosis lesions are not associated with increased lymphocyte infiltration. Mult. Scler. 9, 323–331.
Bo, L., Vedeler, C., Nyland, H., Trapp, B., Mork, S., 2003b. Subpial demyelination in the cerebral cortex of multiple sclerosis patients. J. Neuropathol. Exp. Neurol. 62, 723–732.
Cai, Z., Fan, L., Lin, S., Pang, Y., Rhodes, P., 2011. Intranasal administration of insulin like growth factor-1 protects against lipopolysaccharide-induced injury in the developing rat brain. Neuroscience 194, 195–207.
Calabrese, M., Agosta, F., Rinaldi, F., Mattisi, I., Grossi, P., Favaretto, A., Atzori, M., Bernardi, V., Barachino, L., Rinaldi, L., Perini, P., Gallo, P., Filippi, M., 2009. Cortical lesions and atrophy associated with cognitive impairment in relapsing-remitting multiple sclerosis. Arch. Neurol. 66, 1144–1150.
Calzà, L., Fernandez, M., Giuliani, A., Aloe, L., Giardino, L., 2002. Thyroid hormone activates oligodendrocyte precursor and increases a myelin-forming protein and NGF content in the spinal cord during experimental allergic encephalomyelitis. Proc. Natl. Acad. Sci. 99, 3258–3263.
Calzà, L., Fernandez, M., Giuliani, A., DÍntino, G., Pirondi, S., Sivilia, S., Paradisi, M., DeSordi, N., Giardino, L., 2005. Thyroid hormone and remyelination in adult central nervous system: a lesson from an inflammatory-demyelinating disease. Brain Res. Rev. 48, 339–346.
Calzà, L., Fernandez, M., Giardino, L., 2010. Cellular approaches to central nervous system remyelination stimulation: thyroid hormone to promote myelin repair via endogenous stem and precursor cells. J. Mol. Endocrinol. 44, 13–23.
Cammer, W., Tansey, F., Brosnan, C., 1989. Gliosis in the spinal cords of rats with experimental allergic encephalomyelitis: immunostaining of carbonic anhydrase and vimentin in reactive astrocytes. Glia 2, 223–230.
Cammer, W., Zhang, H., 1992. Carbonic anhydrase in distinct precursors of astrocytes and oligodendrocytes in the forebrains of neonatal and young rats. Brain Res. Dev. Brain Res. 67, 257–263.
Cammer, W., Zhang, H., 1993. Atypical location of the oligodendrocytic isoform (PI) of glutathione-S-transferase in astrocytes during cuprizone intoxication. J. Neurosci. Res. 36, 183–190.
Costa, M., Kessaris, N., Richardson, W., Götz, M., Hedin-Pereira, C., 2007. The marginal zone/layer I as a novel niche for neurogenesis and gliogenesis in developing cerebral cortex. J. Neurosci. 27, 11376–11388.
Dutta, R., Trapp, B., 2007. Pathogenesis of axonal and neuronal damage in multiple sclerosis. Neurology 68, S22–S31.
Dutta, R., Trapp, B., 2011. Mechanisms of neuronal dysfunction and degeneration in Multiple sclerosis. Prog. Neurobiol. 93, 1–12.
Fernandez, M., Giuliani, A., Pirondi, S., D'Intino, G., Giardino, L., Aloe, L., Levi-Montalcini, R., Calzà, L., 2004a. Thyroid hormone administration enhances remyelination in chronic demyelinating inflammatory disease. Proc. Natl. Acad. Sci. 101, 16363–16368.
Fernandez, M., Paradisi, M., Del Vecchio, G., Giardino, L., Calzà, L., 2004b. Thyroid hormone induces glial lineage of primary neurospheres derived from non-pathological and pathological rat brain: implications for remyelination-enhancing therapies. Int. J. Dev. Neurosci. 27, 769–778.
Franco, P., Silvestroff, L., Soto, E., Pasquini, J., 2008. Thyroid hormones promote differentiation of oligodendrocyte progenitor cells and improve remyelination after cuprizone-induced demyelination. Exp. Neurol. 212, 458–467.
Franklin, R., 2003. Why does remyelination fail in multiple sclerosis? Nat. Rev. Neurosci. 3, 705–714.
Franklin, R., Ffrench-Constant, C., 2008. Remyelination in the CNS: from biology to therapy. Nat. Rev. Neurosci. 9, 839–855.
Friesema, E., Ganguly, S., Abdalla, A., Manning Fox, J., Halestrap, A., Visser, T., 2003. Identification of monocarboxylate transporter 8 as a specific thyroid hormone transporter. J. Biol. Chem. 278, 40128–40135.
Girolamo, F., Ferrara, G., Strippoli, M., Rizzi, M., Errede, M., Trojano, M., Perris, R., Roncali, L., Svelto, M., Mennini, T., Virgintino, D., 2011. Cerebral cortex demyelination and oligodendrocyte precursor response to experimental autoimmune encephalomyelitis. Neurobiol. Dis. 43, 678–689.
Gudi, V., Moharregh-Khiabani, D., Skripuletz, T., Koutsoudaki, P., Kotsiari, A., Skuljec, J., Trebst, C., Stangel, M., 2009. Regional differences between grey and white matter in cuprizone induced demyelination. Brain Res. 1283, 127–138.
Harsan, L., Steibel, J., Zaremba, A., Agin, A., Sapin, R., Poulet, P., Guignard, B., Parizel, N., Grucker, D., Boehm, N., Miller, R., Ghandour, M., 2008. Recovery from chronic demyelination by thyroid hormone therapy: myelinogenesis induction and assessment by diffusion tensor magnetic resonance imaging. J. Neurosci. 28, 14189–14201.
Hiremath, M., Saito, Y., Knapp, G., Ting, J., Suzuki, K., Matsushima, G., 1998. Microglia/macrophage accumulation during cuprizone-induced demyelination in C57BL/6 mice. J. Neuroimmunol. 92, 38–49.
Illum, L., 2000. Transport of drugs from the nasal cavity to the central nervous system. Eur. J. Pharm. Sci. 11, 1–18.
Jogani, V., Jinturkar, K., Vyas, T., Misra, A., 2008. Recent patents on intranasal administration for CNS drug delivery. Recent Pat. Drug Deliv. Formul. 2, 25–40.
Kiessling, W., Pflughaupt, K., Haubitz, I., Mertens, H., 1980. Thyroid function in multiple sclerosis. Acta Neurol. Scand. 62, 255–258.
Kinne, A., Schülein, R., Krause, G., 2011. Primary and secondary thyroid hormone transporters. Thyroid. Res. 4 (Suppl. 1), S7.
Kipp, M., Gingele, S., Pott, F., Clarner, T., van der Valk, P., Deneckle, B., Gan, L., Siffrin, V., Zipp, F., Dreher, W., Baumgartner, W., Pfeifenbring, S., Godbout, R., Amor, S., Beyer, C., 2011. BLBP expression in astrocytes during experimental demyelination and in human multiple sclerosis lesions. Brain, Behav. Immun. 25, 1554–1568.
Komoly, S., 2005. Experimental demyelination caused by primary oligodendrocyte dystrophy. Regional distribution of the lesions in the nervous system of mice. Ideggyogy. Sz. 58, 40–43.
Kutzelnigg, A., Lassmann, H., 2005. Cortical lesions and brain atrophy in MS. J. Neurol. Sci. 233, 55–59.
Kutzelnigg, A., Luccinetti, C., Stadelmann, C., Brück, W., Rauschka, H., Bergmann, M., Schmidbauer, M., Parisi, J., Lassmann, H., 2005. Cortical demyelination and diffuse white matter injury in multiple sclerosis. Brain 128, 2705–2712.
Kutzelnigg, A., Faber-Rod, J., Bauer, J., Lucchinetti, C., Sorensen, P., Laursen, H., Stadelmann, C., Brück, W., Rauschka, H., Schmidbauer, M., Lassmann, H., 2007. Widespread demyelination in the cerebellar cortex in multiple sclerosis. Brain Pathol. 17, 38–44.
Love, S., 1988. Cuprizone neurotoxicity in the rat: morphologic observations. J. Neurol. Sci. 84, 223–237.
Ludwin, S., 1978. Central nervous system demyelination and remyelination in the mouse. Lab. Investig. 39, 597–612.
Mangiardi, M., Crawford, D., Xia, X., Du, S., Simon-Freeman, R., Voskuhl, R., Timari-Woodruf, S., 2011. An animal model of cortical and callosal pathology in multiple sclerosis. Brain Pathol. 21, 263–278.

Marta, C., Adamo, A., Soto, E., Pasquini, J., 1998. Sustained neonatal hyperthyroidism in the rat affects myelination in the central nervous system. J. Neurosci. Res. 53, 251–259.

Mason, J., Toews, A., Hostettler, J., Morell, P., Suzuki, K., Goldman, J., Matsushima, G., 2004. Oligodendrocytes and progenitors become progressively depleted within chronically demyelinated lesions. Am. J. Pathol. 164, 1673–1682.

Matsushima, G., Morell, P., 2001. The neurotoxicant Cuprizone as a model to study demyelination and remyelination in the central nervous system. Brain Pathol. 11, 107–116.

Merkus, F., van den Berg, M., 2007. Can nasal drug delivery bypass the blood–brain-barrier? Questioning the direct transport theory. Drugs R&D 8, 133–144.

Munteis, E., Cano, J., Flores, J., Martinez-Rodriguez, J., Miret, M., Roquer, J., 2007. Prevalence of autoimmune thyroid disorders in a Spanish multiple sclerosis cohort. Eur. J. Neurol. 14, 1048–1052.

Niderwiesser, G., Buchinger, W., Bonelli, R., Berghold, A., Reisecker, F., Költringer, P., Archelos, J., 2003. Prevalence of autoimmune thyroiditis and non-immune thyroid disease in multiple sclerosis. J. Neurol. 250, 672–675.

Norton, W., Aquino, D., Hozumi, I., Chiu, F., Brosnan, C., 1992. Quantitative aspects of reactive gliosis: a review. Neurochem. Res. 17, 877–885.

Pasquini, J., Adamo, A., 1994. Thyroid hormones and the central nervous system. Dev. Neurosci. 16, 1–8.

Pathan, S., Iqbal, Z., Zaidi, S., Taleganokar, S., Vohra, D., Jain, G., Azwm, A., Jain, N., Lalani, J., Khar, R., Ahmad, F., 2009. CNS drug delivery systems: novel approaches. Recent Pat. Drug Deliv. Formul. 3, 71–89.

Paxinos, G., Watson, C., 1986. The Rat Brain in Stereotaxic Coordinates, Second Edition. Academic Press, NewYork.

Peterson, J., Bo, L., Mork, S., Chang, A., Trapp, B., 2001. Transected neurites, apoptotic neurons and reduced inflammation in cortical MS lesions. Ann. Neurol. 50, 389–400.

Polman, C., Reingold, S., Edan, G., Filippi, M., Hartung, H., Kappos, L., Lublin, F., Metz, L., McFarland, H., O´Connor, P., Sandberg-Wollheim, M., Thompson, A., Weinshenker, B., Wolinsky, J., 2005. Diagnostic criteria for multiple scerosis: 2005 revisions to the "McDonald Criteria". Ann. Neurol. 58, 840–846.

Polman, C., Reingold, S., Banwell, B., Clanet, M., Cohen, J., Filippi, M., Fujihara, K., Havrdova, E., Hutchinson, M., Kappos, L., Lublin, F., Montalban, X., O´Connor, P., Sandberg-Wollheim, M., Thompson, A., Waubant, E., Weinshenker, B., Wolinsky, J., 2011. Diagnostic criteria for multiple sclerosis: 2010 revisons to the "McDonald Criteria". Ann. Neurol. 69, 292–302.

Rinaldi, F., Calabrese, M., Grossi, P., Puthenparampil, M., Perini, P., Gallo, P., 2010. Cortical lesions ans cognitive impairment in multiple sclerosis. Neurol. Sci. 31 (Suppl. 2), S235–S237.

Roberts, L., Woodford, K., Zhou, M., Black, D., Haggerty, J., Tate, E., Grindstaff, K., Mengesha, W., Raman, C., Zerangue, N., 2008. Expression of the thyroid hormone transporters monocarboxylate transporter-8 (SLC16A2) and organic ion transporter-14 (SLCO1C1) at the blood–brain-barrier. Endocrinology 149, 6251–6261.

Rodríguez-Peña, A., 1999. Oligodendrocyte development and thyroid hormone. J. Neurobiol. 40, 497–512.

Scranton, R., Fletcher, L., Sprague, S., Jimenez, D., Digicaylioglu, M., 2011. The rostral migratory stream plays a key role in intranasal delivery of drugs into the CNS. PLoS One 6 (4), e18711.

Silvestroff, L., Bartucci, S., Soto, E., Pasquini, J., Franco, P., 2010. Cuprizone-induced demyelination in CNP::GFP transgenic mice. J. Comp. Neurol. 518, 2261–2283.

Skripuletz, T., Lindner, M., Kotsiari, A., Garde, N., Fokuhl, J., Linsme-ier, F., Trebst, C., Stangel, M., 2008. Cortical demyelination is prominent in the murine cuprizone model and is strain–dependent. Am. J. Pathol. 172, 1053–10561.

Stidworthy, M., Genoud, S., Suter, U., Mantei, N., Franklin, R., 2003. Quantifying the early stages of remyelination following cuprizone-induced demyelination. Brain Pathol. 13, 329–339.

Storch, M., Bauer, J., Linington, C., Olsson, T., Weissert, R., Lassmann, H., 2006. Cortical demyelination can be modeled in specific rat models of autoimmune encephalomyelitis and is major histocompatibility complex (MHC) haplotype-related. J. Neuropathol. Exp. Neurol. 65, 1137–1142.

Talbott, J., Loy, D., Liu, Y., Qiu, M., Bartlett Bunge, M., Rao, M., Whittemore, S., 2005. Endogenous $Nkx2.2^{+}$/$Olig2^{+}$ oligodendrocyte precursor cells fail to remyelinate the demyelinated adult rat spinal cord in the absence of astrocytes. Exp. Neurol. 192, 11–24.

Tamagno, I., Schiffer, D., 2006. Nestin expression in reactive astrocytes of human pathology. J. Neurooncol. 80, 227–233.

Tani, M., Glabinski, A., Tuohy, V., Stoler, M., Estes, M., Ransohoff, R., 1996. In situ hybridization analysis of glial fibrillary acidic protein mRNA reveals evidence of biphasic astrocyte activation during acute experimental autoimmune encephalomyelitis. Am. J. Pathol. 148, 889–896.

Thorne, R., Pronk, G., Padmanabhan, V., Frey, W., 2004. Delivery of insulin-like growth factor-I to the rat brain and spinal cord along olfactory and trigeminal pathways following intranasal administration. Neuroscience 127, 481–496.

Trapp, B., Nave, K., 2008. Multiple sclerosis: an immune or neurodegenerative disorder ? Annu. Rev. Neurosci. 31, 247–269.

Vucic, S., Burke, T., Lenton, K., Ramanathan, S., Gomes, L., Yannikas, C., Kiernan, M., 2011. Cortical dysfunction underlies disability in multiple sclerosis. Mult. Scler. doi:10.1177/1352458511424308

Wu, Q., Yang, Q., Cate, H., Kemper, D., Binder, M., Wang, H., Fang, K., Quick, M., Marriot, M., Kilpatrick, T., Egan, G., 2008. MRI identification of the rostral-caudal pattern of pathology within the corpus callosum in the cuprizone mouse model. J. Magn. Reson. Imaging 27, 446–453.

Xie, M., Tobin, J., Buddle, M., Chen, C., Trinkaus, K., Cross, A., McDaniel, D., Song, S., Armstrong, R., 2010. Rostrocaudal analysis of corpus callosum demyelination and axon damage across disease stages refines diffusion tensor imaging correlations with pathological features. J. Neuropathol. Exp. Neurol. 69, 704–716.